Electronic Supplementary Material (ESI) for Inorganic Chemistry Frontiers.

Type: Supporting information

Spray-Assisted Deposition of SnO_2 Electron Transport Bilayer for Efficient Inkjet-Printed Perovskite Solar Cells

*Vinayak Vitthal Satale[a], Neetesh Kumar[a], Hock Beng. Lee[a], Manoj Mayaji Ovhal[a], Sagnik Chowdhury[a], Barkha Tyagi[a], Asmaa Mohamed[a], and Jae-Wook Kang[a]**

Dr.Vinayak Vitthal Satale, Dr. Neetesh Kumar, Dr. Hock Beng Lee, Dr. Manoj Mayaji Ovhal, Mr. Sagnik Chowdhury, Dr. Barkha Tyagi, Mrs. Asmaa Mohamed, and Prof. Jae-Wook Kang

[a] Department of Flexible and Printable Electronics, LANL-CBNU Engineering Institute-Korea, Jeonbuk National University, Jeonju 54896, Republic of Korea.

*Corresponding author: Prof. Jae-Wook Kang

E-mail: jwkang@jbnu.ac.kr

Experimental details:

Materials: All of the materials, tin(II) chloride dihydrate ($SnCl_2 \cdot 2H_2O$, 98%, Sigma-Aldrich), lead(II) iodide (PbI_2, 99.99%, TCI Chemicals), formamidinium iodide (FAI, GreatCell Solar), lead bromide ($PbBr_2$, >98%, TCI Chemicals), methylammonium bromide (MABr, GreatCell Solar), cesium iodide (CsI, 99.99%, TCI Chemicals), spiro-oMeTAD (>99%, Lumtech), bis(trifluoromethane)sulfonimide lithium salt (Li-TSFI, 99.95%, Sigma Aldrich), DMF (99.8%, Sigma-Aldrich), dimethyl sulfoxide (DMSO, 99.8%, Sigma-Aldrich), γ-butyrolactone (GBL, Sigma-Aldrich), ethyl acetate (99.5%, Sigma-Aldrich), hexane (99.5%, Sigma-Aldrich), chlorobenzene (99.9%, Sigma-Aldrich), ethanol (99.5%, Merck), 4-tert-butylpyridine (tBP, 96%, Sigma-Aldrich), and acetonitrile (99.8%, Sigma-Aldrich) were used as received without further purification.

Fabrication of different SnO_2-based ETLs: Patterned ITO-coated glass substrates (sheet resistance of ≈8 Ω/□) with dimensions of 2.5 cm × 2.5 cm were ultrasonically washed in acetone, ethanol, and IPA for 10 min each in sequence and then subjected to UV-ozone treatment for 15 min. Three different SnO_2 ETLs were prepared in this study, namely spin-SnO_2, spray-SnO_2, and SnO_2-bilayer. The spin-SnO_2 ETL was prepared by spin-coating the SnO_2 colloidal stock solution, the detailed process was illustrated in previous work.[1] Spray-SnO_2 ETLs were prepared by using the spray technique at room temperature.[2] The fabrication of the SnO_2-bilayer ETL was prepared by spin-coating a precursor solution containing $SnCl_2 \cdot 2H_2O$ in ethanol (23 mg mL^{-1}) at 3000 rpm for 30 s, followed by the annealing treatment at 190 °C in the air for hour. After cooling the substrate was subjected to a UV-ozone treatment for 200 s, then the second layer of

SnO_2 was deposited using the spray technique with the same recipe used for the spray-SnO_2 process.

Perovskite ink preparation: The ink for inkjet printing was prepared as follows: $CH(NH_2)_2I$ (FAI, 0.6 m), PbI_2 (0.66 m), CH_3NH_3Br (MABr, 0.12 m), and $PbBr_2$ (0.12 m) were dissolved in a mixture of DMF, DMSO, and GBL in a ratio of 28:26:46 (volume percentage). Additionally, CsI (1.5 m, Alfa Aesar) was dissolved in DMSO and then added to the first solution to produce a 0.75 m TCP solution with the composition $Cs_{0.10}FA_{0.75}MA_{0.15}Pb(Br_{0.15}I_{0.85})_3$. Before printing, the ink was filtered with a 0.45 µm pore size polytetrafluoroethylene (PTFE) filter.

Inkjet-printed PSC device fabrication: For inkjet printing of the perovskite layer, an inkjet printer (Dimatix Fujifilm, DMP-2800) with a print head module for 2.4 pL cartridges (SAMBA, 12 nozzles) was used. Before printing, the SnO_2 surface was treated with oxygen plasma at low power for 200 s. For printing, a jetting frequency of 5 kHz was used together with a single pulse waveform with a peak voltage of 28 V and a pulse width of 5 µs with a drop spacing of 17 µm. The total area of inkjet-printed TCP was 23x15 mm² per sample. Within the 30 s, the as-printed samples were manually moved to a nearby vacuum chamber which was evacuated down to about 5-7 x 10^{-3} Torr. Then, the chamber was slowly vented, and the samples were annealed on a hotplate at 100 °C for 1 h. The complete printing procedure was done in a controlled ambient atmosphere (≈23 °C, ≈40% relative humidity) in a clean room. For spin coating of the TCP layers, the SnO_2 samples were also treated with oxygen plasma for 200 s. The TCP layer was spin-coated using a two-step program (1000 rpm for 12 s, 3000 rpm for 32 s) and drifted the antisolvent (100 µL) solution prepared by mixing ethyl acetate (EA) and hexane (Hex) in 7:3 v/v, and then annealed for 1 h on a hotplate at 100 °C. The 2,2',7,7'-Tetrakis [N, N-di(4-

methoxyphenyl) amino]-9,9'-spirobifluorene (Spiro-OMeTAD) was deposited onto the perovskite film by spin-coating 30 µL of the mixed solution, which contained 72.3 mg of spiro-OMeTAD salt in 1 mL of chlorobenzene, doped with 30 µL of 4-tert-Butylphenol, and 35 µL of Lithium bis(trifluoromethane sulfonyl) imide solution (260 mg in 1 mL of acetonitrile). Finally, a ≈120 nm Ag contact was thermally evaporated as the top electrode using a shadow mask (aperture area: 0.09 cm^2).

Characterization:

The surface morphology and topography of the different SnO_2 films and perovskite films were characterized using an FE-SEM (Carl Zeiss, SUPRA40VP) and an AFM (Park Systems, NX-10) installed in the Center for University-Wide Research Facilities (CURF) at Jeonbuk National University. The crystallographic changes of the SnO_2 films were characterized by an X-ray diffractometer (Bruker D8 Advance) using CuKα excitation, also located at the aforementioned facility. The optical transmittance and absorption of the SnO_2 films were measured (wavelength range 300-850 nm) using a UV–vis spectrophotometer (PerkinElmer Lambda 750), and the steady-state photoluminescence spectra of the SnO_2/perovskite samples were obtained from a photoluminescence spectrometer (Horiba FluoroMax-4). Wettability tests over the SnO_2 samples were performed using the Surface electro-optics (Phoenix 300 Touch, Kromtek) automatic contact angle analyzer with a water drop volume of 1 µL. The XPS depth profile measurements were conducted using a Nexsa XPS system (ThermoFisher Scientific, UK). The measurement conditions were X-ray source: monochromatic Al-Kα (1486.6 eV), base pressure: 1.0×10^{-8} Torr, beam size: 400 µm, and depth profile: Ar monatomic 1keV. The TRPL measurements for the perovskite films were executed using an inverted-type scanning confocal microscope

(MicroTime-200, Pi coQuant, Germany) with a 4 × (air) objective, using a single-mode pulsed diode laser as an excitation source (wavelength: 470 nm, pulse width: 30 ps, and average power: ≈100 nW in 200 kHz repetition rate). For the PSC device characterization, the current density–voltage (J–V) measurements were conducted using a Keithley 2400 source meter under a simulated one-sun illumination (100 mW cm^{-2}; AM 1.5G standard) from an Oriel Sol 3A solar simulator (Newport Inc.). Before conducting the measurements, the system was calibrated against an NREL-certified reference solar cell. The device area was 0.09 cm^2 and defined by the shadow masks. The EQE spectra of the PSCs were acquired using an Oriel quantum efficiency measurement device (IQE-200).

Estimation of Oxygen defects in ETLs:

Table S1. The atomic percentage of the subcomponents in O1s core-level spectra of spin-SnO_2, spray-SnO_2, and Bi-SnO_2 samples.

Sample	The area under the subpeaks						
	O_1	O_2	O_3	O_{Total}	$O_{lattice}$ $[O_1/O_{Total}]$	$O_{defects}$ $[(O_2+O_3)/O_{Total}]$	$[O_{defects}/O_{lattice}]$
Spin-SnO_2	351026	108004	37306	496336	0.7072	0.2927	0.4139
Spray-SnO_2	359167	86044	29377	474588	0.7568	0.2432	0.3214
SnO_2 bilayer	375980	78202	27902	482024	0.7799	0.2201	0.2823

AFM study of inkjet-printed Perovskite films:

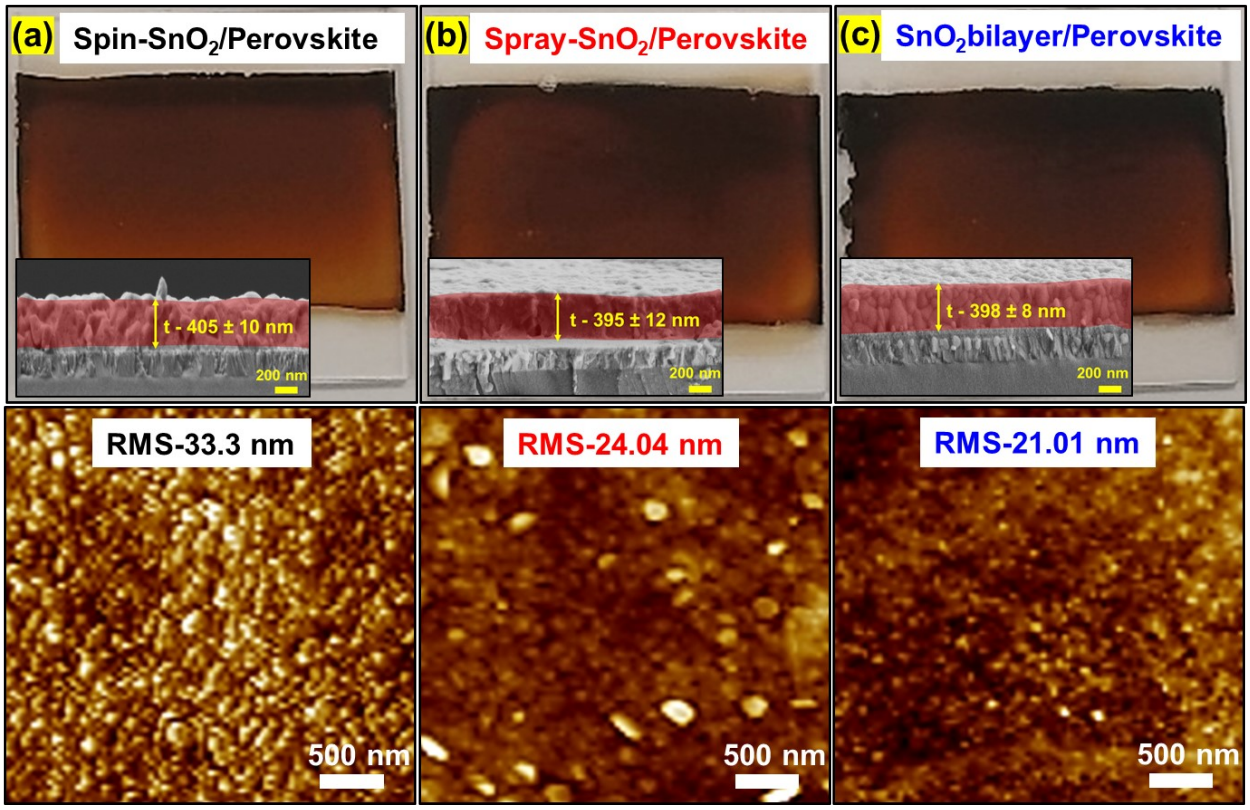

Figure S1- Digital photographs and FE-SEM cross-sectional images of inkjet perovskite films coated on different ETLs and corresponding atomic force microscope (AFM) topographic images of the perovskite layers fabricated on top of the spin (a), spray (b), and SnO_2 bilayer (c) ETLs.

XPS study of inkjet-printed perovskite:

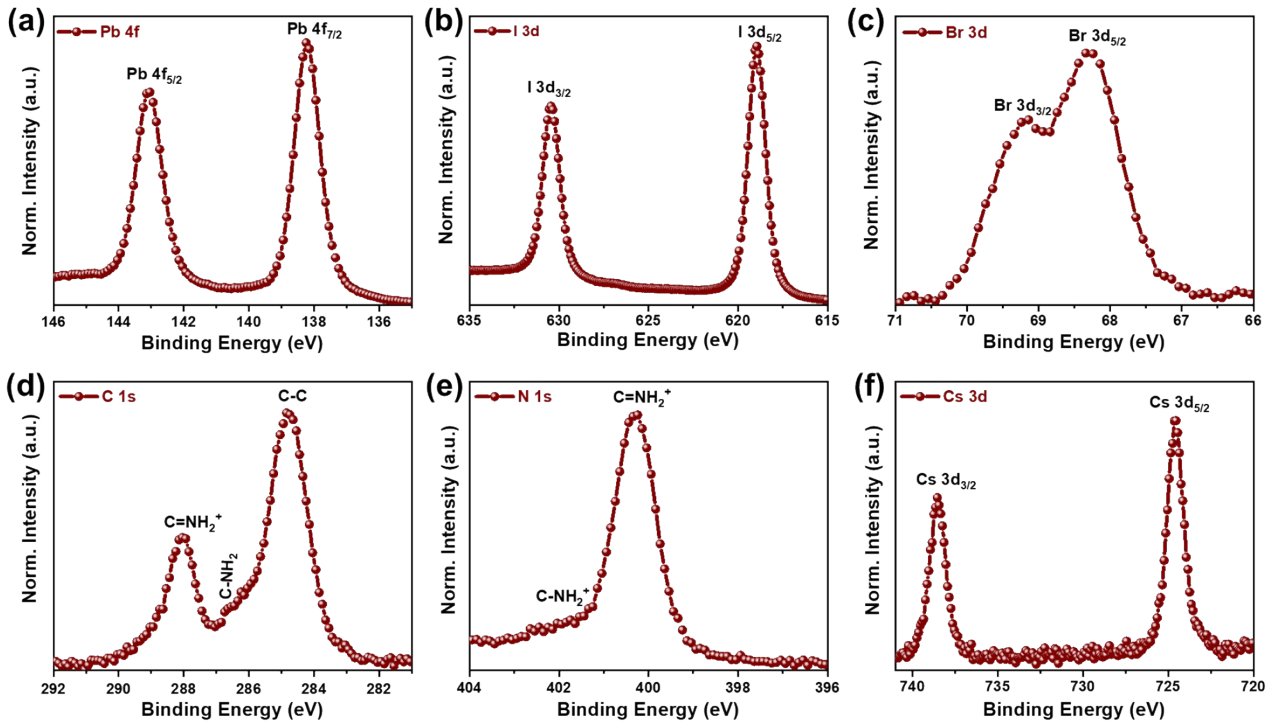

Figure S2- (a) Pb 4f, (b) I 3d, (c) Br 3d, (d) C 1s, (e) N 1s, and (f) Cs 3d core-level X-ray photoelectron spectroscopy (XPS) spectra of perovskite film.

Estimation of UPS parameters:

***Optical band gap (E_g)** was obtained from the optical absorption spectra using the Tauc relationship.

Work function W_S (*eV*) = 21.22 eV – $E_{cut\text{-}off}$ (eV) ..... (Exp.S1)
E_{VBM} (eV) = W_S (eV) + E_{onset} (eV) ..... (Exp.S2)
Conduction band E_C (eV) = Ws (eV) + E_{VBM} (eV) – E_g (eV) ..... (Exp.S3)

Table S2. Detailed band structure parameters derived from the UPS and absorption spectra of all SnO_2 and perovskite films.

Sample	$E_{on\text{-}set}$ (eV)	$E_{cut\text{-}offt}$ (eV)	E_g (eV)	W_s (eV)	E_{VBM} (eV)	E_C (eV)
Spin-SnO_2	3.93	17.53	3.69	3.69	7.62	3.93
Spray-SnO_2	3.97	17.5	3.61	3.72	7.69	4.08
SnO_2 bilayer	3.94	17.32	3.59	3.90	7.84	4.25
Perovskite	1.54	16.98	1.65	4.24	5.78	4.13

J-V study for spin-coated perovskite:

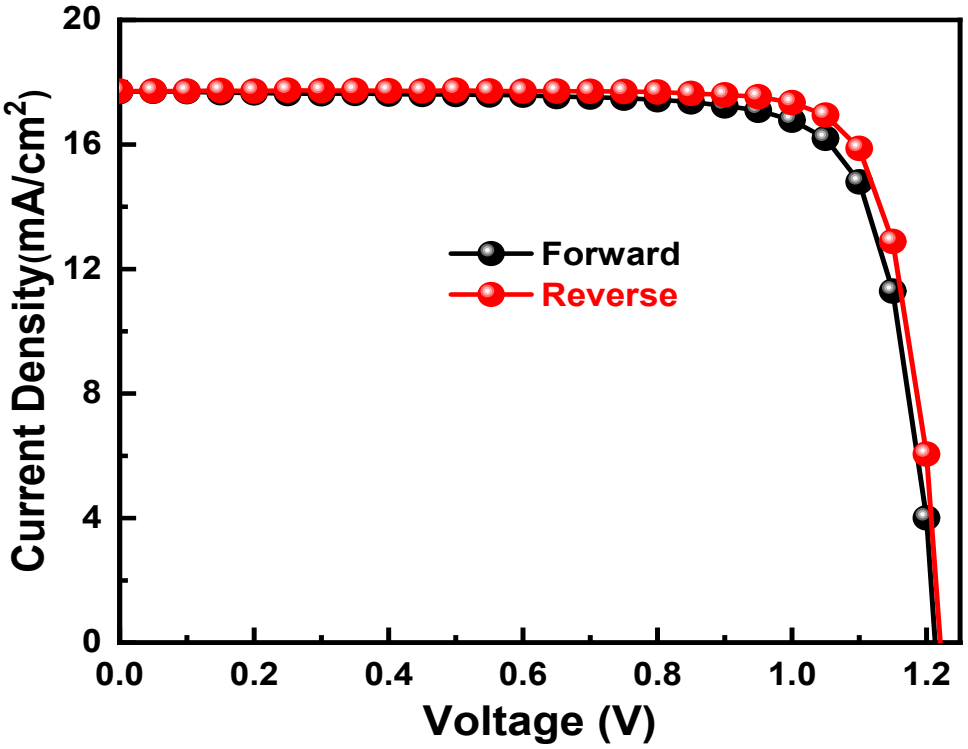

Figure S3: J–V characteristic curves of PSC devices based on spin-SnO_2 ETL and spin-coated perovskite in the forward and reverse scan directions.

Table S3. Performance of spin-coated PSCs.

Device	V_{OC} (V)	J_{SC} (mA/cm^2)	Fill Factor (%)	Efficiency (%)
Forward	1.213	17.71	79.16	17.01
Reverse	1.220	17.73	82.31	17.81
Average	1.221	17.71	79.71	17.23

Hysteresis Index Calculation:

The hysteresis effect of the PSC device can be quantified using a dimensionless hysteresis index (HI) expression below.

$$HI = \frac{PCE_{RS} - PCE_{FS}}{PCE_{RS}} \quad \text{..... (Exp. S4)}$$

Here, PSC_{FS} represents the photocurrent in forward-bias scanning, whereas PSC_{RS} represents the photocurrent at bias in reverse-bias scanning.

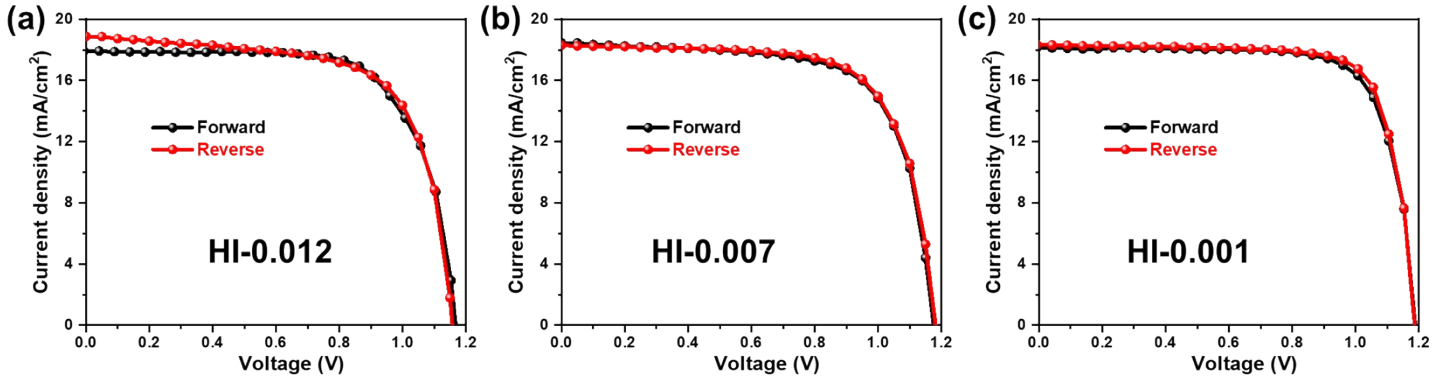

Figure S4- J–V characteristic curves of the representative inkjet-printed PSCs based on different ETLs (a) Spin-SnO_2, (b) spray-SnO_2, and (c) SnO_2 bilayer in the forward and reverse scan directions.

Stabilized current density at maximum power point:

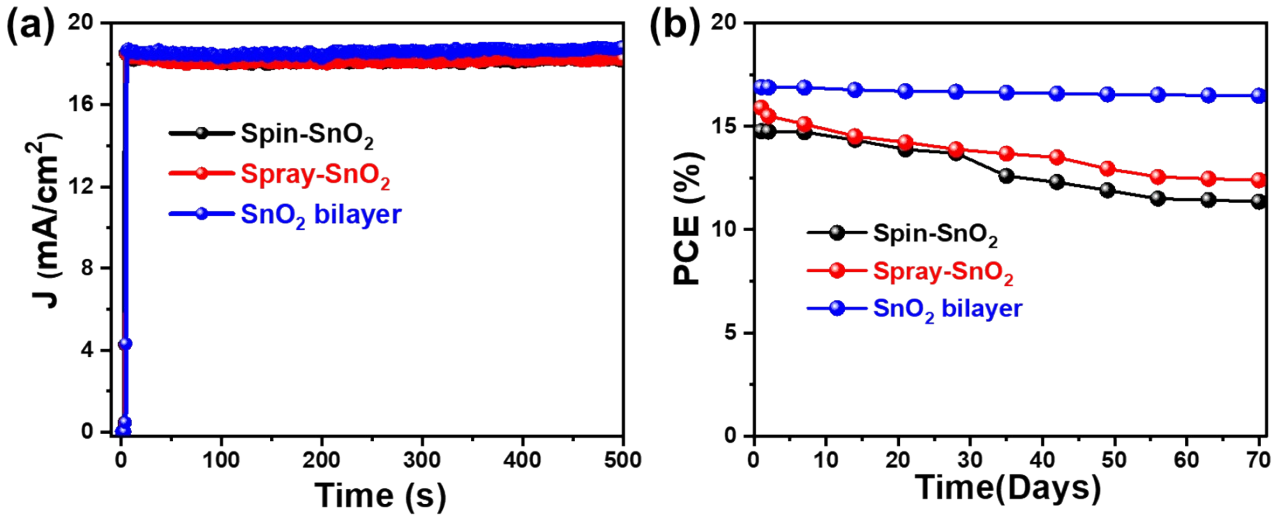

Figure S5. (a) A steady-state current density of the inkjet-printed PSC devices measured at the maximum power point. (b) The device stability study for IJP PSCs stored under ambient conditions (temp: 25–30°C; RH: 30–35%).

Estimation of Fluorescence decay lifetimes:

The equation used for tri-exponential curve fitting of the TRPL curve:

$$\tau_{PL} = \frac{A_1\tau_1^3 + A_2\tau_2^3 + A_3\tau_3^3}{A_1\tau_1 + A_2\tau_2 + A_3\tau_3} \qquad \text{.....(Exp. S5)}$$

Here, A_1, A_2, and A_3 are the relative weight fraction amplitudes; and τ_1, τ_2, and τ_3 are fast and slow fluorescence decay lifetimes

Table S4. The average fluorescence decay lifetime of perovskite films is based on the bi-exponential fitting of TRPL spectra.

Sample	A_1 (kCnts)	τ_1 (ns)	A_2 (kCnts)	τ_2 (ns)	A_3 (kCnts)	τ_3 (ns)	$\tau_{average}$ (ns)
Perovskite	1.1	82	2.85	30	5.9	1.9	54
Spin-SnO_2/Perovskite	1.73	62	2.96	24	5.49	2.38	44
Spray-SnO_2/Perovskite	1.27	57	3.11	22	5.5	2	37
SnO_2 -bilayer/Perovskite	0.72	48	5.33	19	3.5	2.2	25

Performance comparison with previous literature:

Table S5. A comparison of inkjet-printed PSC device performance based on different ETLs with various perovskite systems was reported in the literature.

Device structure	Perovskite material	ETL fabrication method	PCE (%)	Reference
FTO/TiO_2/ Perovskite/C	$CH_3NH_3PbI_3$	Spin	11.60	3
FTO/TiO_2/Perovskite/Spiro-MeOTAD/Au		Spin	12.3	4
FTO/TiO_2/ZrO_2/Perovskite /Spiro-MeOTAD/Au		Spray	9.53	5
FTO/TiO_2/Perovskite /Spiro-MeOTAD/Au		Spin	6.80	6
FTO/TiO_2/Perovskite /Spiro-MeOTAD/Au	$FA_{0.15}MA_{0.85}PbI_{2.55}Br_{0.45}$	IJP	14.11	7
FTO/TiO_2/C_{60}/Perovskite /Spiro-MeOTAD/Au	$CH_3NH_3PbI_3$	Dip	17.04	8
FTO/TiO_2/Perovskite /Spiro-MeOTAD/Au		Spin	18.20	9
FTO/TiO_2/Perovskite /Spiro-MeOTAD/Au	$Cs_{0.1}(FA_{0.83}MA_{0.17})_{0.9}Pb(Br_{0.17}I_{0.83})_3$	Spin	11.50	10
FTO/TiO_2/C_{60}/Perovskite /Spiro-MeOTAD/Au	$Cs_{0.05}MA_{0.14}FA_{0.81}PbI_{2.55}Br_{0.45}$	Dip	19.60	11
FTO/TiO_2/Perovskite /C	$CH_3NH_3PbI_3$	IJP	12.07	12
ITO/SnO_2/Perovskite + PTB7 /Spiro-MeOTAD/Au	$Cs_{0.05}FA_{0.79}MA_{0.16}Pb(Br_{0.17}I_{0.83})_3$	Spin	10.35	13
ITO/Spin-SnO_2/Perovskite/Spiro-MeOTAD/Ag	**$Cs_{0.10}FA_{0.75}MA_{0.15}Pb(Br_{0.15}I_{0.85})_3$**	**Spin**	**14.77**	**This work**
ITO/Spray-SnO_2/Perovskite/Spiro-MeOTAD/Ag		**Spray**	**15.29**	
ITO/SnO_2 bilayer/Perovskite/Spiro-MeOTAD/Ag		**Spin/spray**	**16.90**	

Reference:

1 H. B. Lee, N. Kumar, M. M. Ovhal, Y. J. Kim, Y. M. Song and J.-W. Kang, Dopant-free, amorphous–crystalline heterophase SnO_2 electron transport bilayer enables >20% efficiency in triple-cation perovskite solar cells, *Adv. Funct. Mater.*, 2020, **30**, 2001559.

2 K. Neetesh, H. B. Lee, R. Sahani, B. Tyagi, S. Cho, J.-S. Lee and J.-W. Kang, Room-temperature spray deposition of large-area SnO_2 electron transport layer for high performance, stable $FAPbI_3$-based perovskite solar cells, *small methods*, 2022, **6**, 2101127.

3 Z. Wei, H. Chen, K. Yan and S. Yang, Inkjet printing and instant chemical transformation of a CH3NH3PbI3/nanocarbon electrode and interface for planar perovskite solar cells, *Angew. Chemie - Int. Ed.*, 2014, **53**, 13239–13243.

4 S. G. Li, K. J. Jiang, M. J. Su, X. P. Cui, J. H. Huang, Q. Q. Zhang, X. Q. Zhou, L. M. Yang and Y. L. Song, Inkjet printing of $CH_3NH_3PbI_3$ on a mesoscopic TiO_2 film for highly efficient perovskite solar cells, *J. Mater. Chem. A*, 2015, **3**, 9092–9097.

5 S. G. Hashmi, D. Martineau, X. Li, M. Ozkan, A. Tiihonen, M. I. Dar, T. Sarikka, S. M. Zakeeruddin, J. Paltakari, P. D. Lund and M. Grätzel, Air processed inkjet infiltrated carbon based printed perovskite solar cells with high stability and reproducibility, *Adv. Mater. Technol.*, 2017, **2**, 4–9.

6 T. Abzieher, F. Mathies, M. Hetterich, A. Welle, D. Gerthsen, U. Lemmer, U. W. Paetzold and M. Powalla, Additive-assisted crystallization dynamics in two-step fabrication of

perovskite solar cells, *Phys. Status Solidi A*, 2017, **214**, 1700509.

7 A. J. Huckaba, O. Lee, R. Xia, S. Paek, V. C. Bassetto, E. Oveisi, A. Lesch, S. Kinge, P. J. Dyson, H. Girault and N. M. Khaja, Inkjet-printed mesoporous TiO_2 and perovskite layers for high efficiency perovskite solar cells, *Energy Technol.*, 2019, **7**, 317–324.

8 C. Liang, P. Li, H. Gu, Y. Zhang, F. Li, Y. Song, G. Shao, N. Mathews and G. Xing, One-step inkjet printed perovskite in air for efficient light harvesting, *Sol. RRL*, 2018, **2**, 1700217.

9 P. Li, C. Liang, B. Bao, Y. Li, X. Hu, Y. Wang, Y. Zhang, F. Li, G. Shao and Y. Song, Inkjet manipulated homogeneous large size perovskite grains for efficient and large-area perovskite solar cells, *Nano Energy*, 2018, **46**, 203–211.

10 S. Schlisske, F. Mathies, D. Busko, N. Strobel, T. Rödlmeier, B. S. Richards, U. Lemmer, U. W. Paetzold, G. Hernandez-Sosa and E. Klampaftis, Design and color flexibility for inkjet-printed perovskite photovoltaics, *ACS Appl. Energy Mater.*, 2019, **2**, 764–769.

11 Z. Li, P. Li, G. Chen, Y. Cheng, X. Pi, X. Yu, D. Yang, L. Han, Y. Zhang and Y. Song, Ink engineering of inkjet printing perovskite, *ACS Appl. Mater. Interfaces*, 2020, **12**, 39082–39091.

12 D. A. Chalkias, A. Mourtzikou, G. Katsagounos, A. Karavioti, A. N. Kalarakis and E. Stathatos, Suppression of coffee-ring effect in air-processed inkjet-printed perovskite layer toward the fabrication of efficient large-sized all-printed photovoltaics: A perovskite precursor ink concentration regulation strategy, *Sol. RRL*, 2022, 2200196.

13 C. S. Pathak, G. Paramasivam, F. Mathies, K. Hirselandt, V. Schröder, O. Maus, J. Dagar, C. Klimm, E. Unger and I. Visoly-Fisher, Ink-additive for spin-coated versus inkjet-printed perovskite solar cells, *ACS Appl. Energy Mater.*, 2022, **5**, 4085–4095.